Experimental validation of float array tidal current measurements in Agate Pass, WA

Trevor W Harrison,[a] Nate Clemett,[a] Brian Polagye,[a] Jim Thomson,[a]

[a] *University of Washington*

Corresponding author: Trevor W Harrison, twharr@uw.edu

Early Online Release: This preliminary version has been accepted for publication in *Journal of Atmospheric and Oceanic Technology*, may be fully cited, and has been assigned DOI 10.1175/JTECH-D-22-0034.1. The final typeset copyedited article will replace the EOR at the above DOI when it is published.

ABSTRACT: Tidal currents, particularly in narrow channels, can be challenging to characterize due to high current speeds (> 1 m s^{-1}), strong spatial gradients, and relatively short synoptic windows. To assess tidal currents in Agate Pass, WA, we cross-evaluated data products from an array of acoustically-tracked underwater floats and from acoustic Doppler current profilers (ADCPs) in both station-keeping and drifting modes. While increasingly used in basin-scale science, underwater floats have seen limited use in coastal environments. This study presents the first application of a float array towards small-scale (< 1 km), high resolution (< 5 m) measurements of mean currents in energetic tidal channel and utilizes a new prototype float, the μFloat, designed specifically for sampling in dynamic coastal waters. We show that a float array (20 floats) can provide data with similar quality to ADCPs, with measurements of horizontal velocity differing by less than 10% of nominal velocity, except during periods of low flow (0.1 m s^{-1}). Additionally, floats provided measurements of the three dimensional temperature field, demonstrating their unique ability to simultaneously resolve *in situ* properties that cannot be remotely observed.

Accepted for publication in *Journal of Atmospheric and Oceanic Technology*. DOI 10.1175/JTECH-D-22-0034.1.

Significance Statement

The purpose of this research was to validate measurements of tidal currents in a fast-flowing tidal channel using a prototype technology composed of twenty drifting underwater sensors called μFloats ("microFloats") and five surface buoys against standard devices (acoustic Doppler current profilers). Float measurements matched those from the standard devices within 10% of the mean water speed and simultaneously provided three-dimensional mapping of temperature in the test region. Results demonstrate how moderate numbers of simultaneously deployed μFloats can provide high-resolution sensing capacity that will improve our understanding of physical, chemical, and biological processes in coastal waters.

1. Introduction

Tidal currents play a central role in our coastal waters, impacting water quality (Deppe et al. 2013; Defne and Ganju 2015), larval transport (Mahadevan 2016), algae blooms (Livingston 2000), marine navigation (Cheng and Smith 1998; Chen et al. 2013), and energy production (Blunden and Bahaj 2007; Polagye and Thomson 2013). Driven by astronomical forcing, tides are predictable on a decadal time scale, however, the resulting water movements are less predictable (Godin 1983). Local bathymetry can produce currents exceeding 4 m s^{-1}, strong horizontal and vertical heterogeneity, and significant variability over a matter of minutes (McCaffrey et al. 2015). Waterway management, ecosystem health monitoring, and improved scientific understanding all benefit from accurate characterization of local currents on horizontal spatial scales O(0.1-10) km, vertical scales O(0.1-100) m, and time evolution from O(minutes to months).

Since their introduction in the early 1980s, acoustic Doppler current profilers (ADCPs) have become the standard instrument for measuring water velocity (Dickey et al. 1998). ADCPs produce estimates of 3D velocity at discrete distances from the instrument head by emitting a ping from three to five diverging transducers and measuring the Doppler shift on echoes returned from scattering sources in the water (e.g., particulate, bubbles) (Teledyne RDI 2019). A flexible instrument, ADCPs have been deployed on stationary platforms such as bottom-landers (Guerra et al. 2017) and moored buoys (Mayer et al. 2007), as well as on mobile platforms such as autonomous underwater vehicles (An et al. 2001; Brown et al. 2011; Mullison et al. 2011; Todd et al. 2017), vessels (Geyer and Signell 1990; Willcox et al. 2001), and drifting surface-buoys (Guerra and

Thomson 2016; Shcherbina et al. 2018; Guerra et al. 2021). Stationary deployments provide long-duration O(days to months) time-series essential for extracting tidal harmonic constituents at a given site (Foreman et al. 1995; Polagye and Thomson 2013; Jin et al. 2018). However, the spatial coverage of this strategy is limited. Conversely, mobile deployments can map horizontal variations in water velocity (Geyer and Signell 1990), though they are time-limited to O(hours to days). Corrections for platform motion such as translation velocity or heave can be achieved via bottom tracking (i.e., using acoustic reflections from the seafloor to estimate and account for horizontal instrument velocity) and/or through integration with GPS and inertial measurement units. Such correction techniques are commonly included in commercial systems (Muste et al. 2004; Fong and Monismith 2004; Heitsenrether et al. 2018; Velasco and Nylund 2019). Doppler noise can also reduce accuracy, but is addressed by averaging multiple independent samples (Lu and Lueck 1999; Teledyne RDI 2019). For stationary platforms, this is an effective solution, but for mobile platforms, averaging convolves spatial and temporal variability, resulting in a direct trade-off between spatial coverage and accuracy.

Underwater floats have a long history in oceanography (Gould 2005). The Argo program, with nearly 4000 floats distributed worldwide, and over a million profiles taken over the 20 year program history, has provided incomparable data on ocean state variables (salinity, pressure, and temperature), as well as unprecedented resolution of ocean circulation patterns (Jayne et al. 2017). Given the demonstrated success for basin-scale problems, there is growing interest in extending this distributed sensing paradigm to smaller-scale coastal processes. To meet this need, a number of new buoyancy-controlled floats have been developed specifically to operate in the stronger density gradients, shallow and variable bathymetry, and faster currents present in coastal environments (McGilvray and Roman 2010; Roman et al. 2011; Jaffe et al. 2017). For example, Jaffe's group deployed an array to measure larval dispersion resulting from interactions with internal waves (Jaffe et al. 2017; Garwood et al. 2020) and Roman's group developed a system with increased actuation and bottom-tracking ability for coastal bathymetric surveys (McGilvray and Roman 2010; Roman et al. 2011). In Harrison et al. (2020), virtual experiments comparing float arrays and mobile ADCP surveys suggested that float arrays may provide similar accuracy when performing three-dimensional mapping of horizontal water velocity while simultaneously gathering *in situ* water

Accepted for publication in *Journal of Atmospheric and Oceanic Technology*. DOI 10.1175/JTECH-D-22-0034.1.

property data (e.g., temperature, salinity, dissolved oxygen). Encouraged by that result, Harrison et al. (2022) developed the μFloat system to investigate this observational paradigm in practice.

This paper presents an experimental comparison of three-dimensional measurements of horizontal water velocity produced by a μFloat array ($\sim$ 20 floats) to data from four drifting, downward-looking ADCPs and a station-keeping, vessel-mounted ADCP. Section 2 describes the test site, equipment, and data processing methods. Section 3 presents the observed site characteristics and comparisons across platforms. Implications of the outcomes are discussed in Section 4.

2. Methods

a. Site Description

Agate Pass, WA (Fig. 1a,b) is a tidal channel in Puget Sound, WA, bordered on the south by Bainbridge Island and on the north by the Kitsap Peninsula. The channel connects Port Madison, a bay (40-60 m deep) that is part of the main basin of Puget Sound, to Port Orchard, a shallower (20-30 m deep) strait separating Bainbridge Island from the Kitsap Peninsula. Tides in the region are mixed semi-diurnal, with water level ranges reaching 4 m in Port Madison. At its narrowest point, Agate Pass is only 300 m wide and 9 m deep, and produces currents that exceed 2 m s^{-1} during periods of peak exchange. As a result of these high flow speeds, the site is of interest for tidal energy development, which motivated its selection for this study.

b. Instruments

1) Vessel-Mounted ADCP

Fig. 2a depicts the RDI Workhorse Mariner (1200 kHz) four-beam ADCP mounted on a pole for deployment. Five-minute station-keeping surveys at three locations (Fig. 1b, SK1-3) were repeated during each deployment period. During these surveys, the vessel operator held station to within 50 m of the target location. To compensate for residual motion, the RDI VMDAS software integrated bottom track velocities from the ADCP to convert the measurements from a moving reference frame into a fixed reference frame. Ancillary GPS data recorded in VMDAS were integrated to provide positions and timestamps for the measurements. The raw ADCP data were sampled at 2 Hz and assembled into 15-second ensemble profiles. These profiles were screened to retain broadband Doppler correlations above 50% and trimmed to remove spurious values below the seafloor based

Accepted for publication in *Journal of Atmospheric and Oceanic Technology*. DOI 10.1175/JTECH-D-22-0034.1.

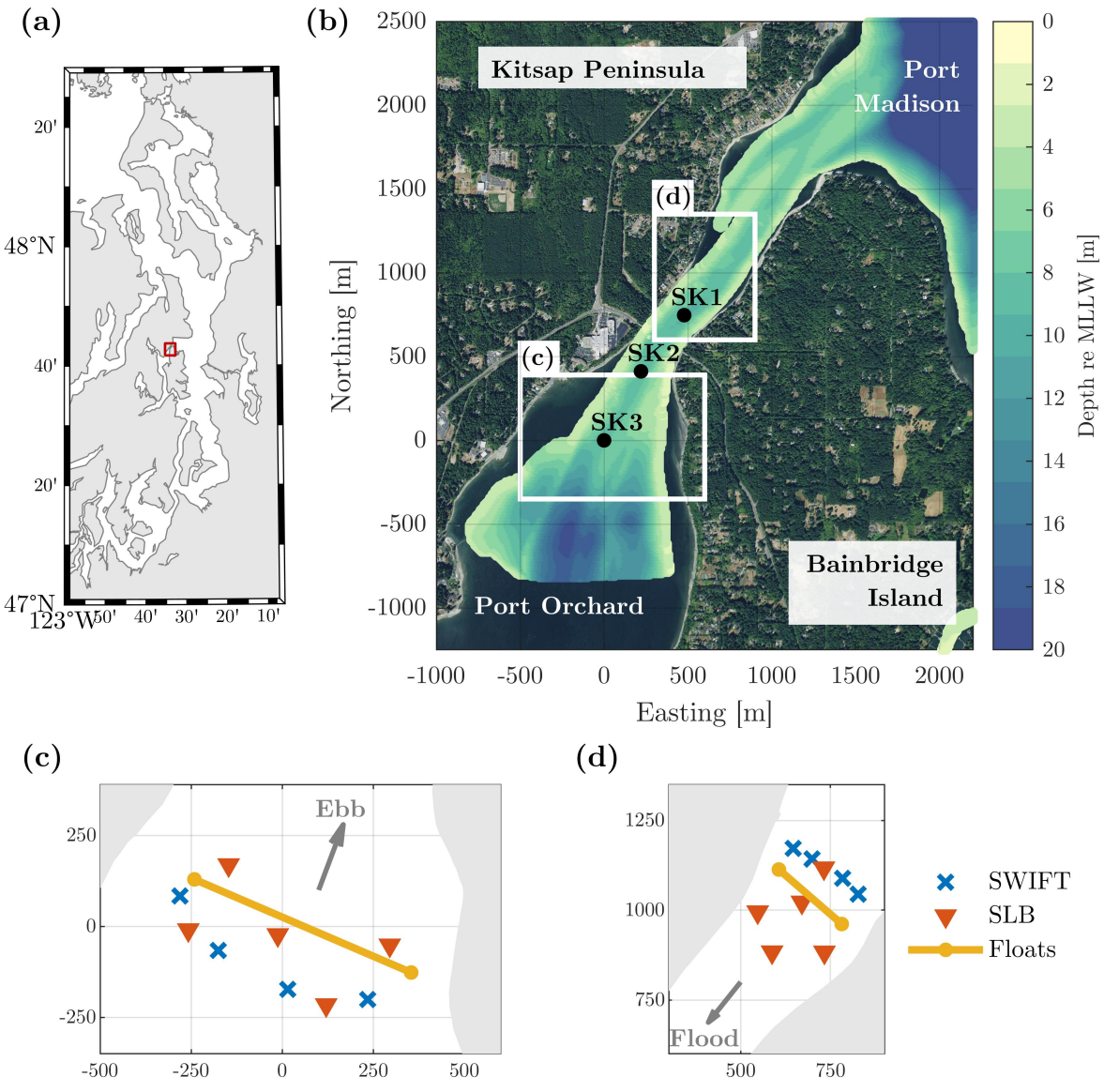

FIG. 1. Map of Puget Sound (a) and Agate Pass, WA (b). Station-keeping (SK) locations are indicated in (b) and remained the same during ebb and flood. (c) and (d) depict initial drifting instrument positions during ebb and flood, respectively, with ~20 μFloats deployed at regular intervals along the indicated line.

on bottom-tracking depth. The ensemble horizontal velocity uncertainty was 0.017 m s^{-1}. For each station and survey cycle, we compute the mean of all ensemble profiles taken within 25 m of the nominal station-keeping location, typically 20-30 total profiles over 5-7 minutes, as well as the standard deviation of these profiles as a measure of local variability. This short-term station-

Accepted for publication in *Journal of Atmospheric and Oceanic Technology*. DOI 10.1175/JTECH-D-22-0034.1.

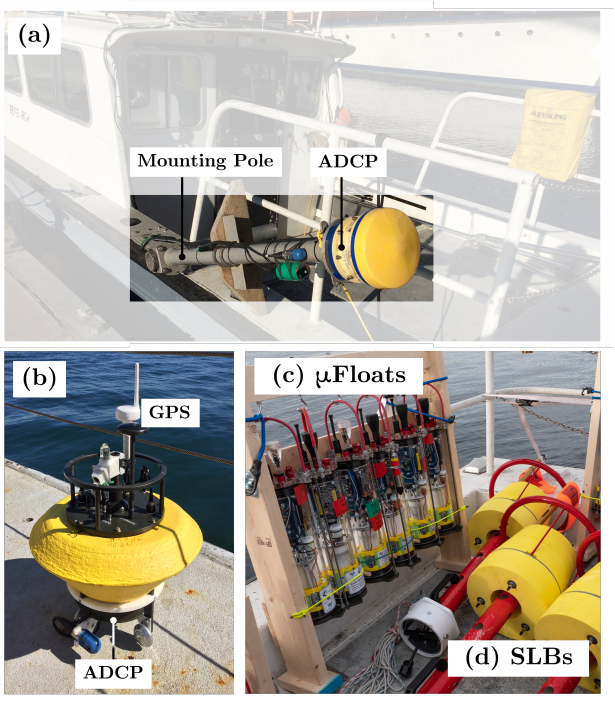

FIG. 2. Primary instruments used in this survey: a vessel-mounted ADCP (a), four SWIFTs (b), twenty μFloats (c), five surface localization buoys (SLBs) (d).

keeping strategy provided sufficient samples to reduce Doppler noise in the ensemble averages, while allowing moderate horizontal coverage (Palodichuk et al. 2013).

2) SWIFTs

The SWIFT (Fig. 2b) is a drifting surface buoy equipped with a downward-facing Nortek Signature1000 five-beam ADCP, Sutron Xpert data logger and processing board, and SBG Ellipse GPS and inertial navigation system (INS) (Thomson 2012; Thomson et al. 2019). An Airmar WX200 provides supplementary wind speed and direction. The ADCP collected 1 Hz data in broadband mode during 512 s bursts. These repeated every 720 s (i.e., 5 bursts per hour), with the intermediary period used for onboard processing of the ADCP data. The ADCP was configured to collect data in 40 depth bins with a resolution of 0.5 m and a 0.35 m blanking distance. In post-processing, the drift velocity of the buoy was added to the observed profiles to estimate the true velocity profile in a fixed reference frame. The velocity profiles were trimmed to remove values beyond the seafloor using an altimeter return from the center beam. Then, 30-second

Accepted for publication in *Journal of Atmospheric and Oceanic Technology*. DOI 10.1175/JTECH-D-22-0034.1.

ensemble averages of the drift-corrected profiles were calculated, resulting in effective uncertainty of 0.005 m s^{-1} (Guerra and Thomson 2017). We note that for the highest drift speed of 2 m s^{-1}, the ensembles effectively average over 60 m of along-track positions.

3) μFloats and Surface Localization Buoys

The μFloat (Fig. 2c) is a prototype underwater float developed specifically for coastal environments (Harrison et al. 2022). Equipped with a solid-piston buoyancy engine, the float can change its density by 9%, providing vertical actuation speeds of ± 0.5 m s^{-1} and depth-holding accuracy within ±20 cm in quiescent water. Primary sensors include pressure (used for depth control), temperature, and an inertial measurement unit (IMU). The large buoyancy engine capacity allows for the addition of external sensors with minimal re-ballasting. When on the surface, the μFloats broadcast their GPS location via cellular and radio signals to facilitate recovery.

An array of five GPS-equipped surface localization buoys (SLBs) are deployed concurrently to track the μFloats while underwater (Fig. 2d). SLBs and μFloats are equipped with small acoustic "nanomodems" (Fenucci et al. 2018; Neasham 2018). The surface buoys broadcast uniquely coded pings on a round-robin schedule. All nanomodems within range record and timestamp these pings. In post-processing, sent and received pings are aligned and time-of-flight is calculated from the associated time stamps. Distances between each source and receiver are then estimated based on sound speed. Sets of three or more pings from unique surface buoys are used to trilaterate float position (Norrdine 2012). Position data are smoothed by a robust moving local regression with a moving window size between 60 and 240 seconds, adjusted for each float depending on ping connectivity rates to ensure that at least 80% of the regression windows along the track included a minimum of 10 individual position points. Velocity is estimated by a first-order central-difference of smoothed position data. Resulting position and velocity uncertainty is ± 15 m and ± 0.06 m s^{-1} respectively. Additional details on the localization process are presented in Harrison et al. (2022). To provide an apples-to-apples comparison with SWIFT data, we subsequently apply the same 30-second ensemble averaging procedure to the float and SLB tracks, reducing position and velocity uncertainty to ~ 3 m and ~ 0.01 m s^{-1}.

During each survey cycle, between 18 and 20 floats were deployed. Two floats were lost during the experiment, with one subsequently recovered. For a given deployment, all floats were programmed

Accepted for publication in *Journal of Atmospheric and Oceanic Technology*. DOI 10.1175/JTECH-D-22-0034.1.

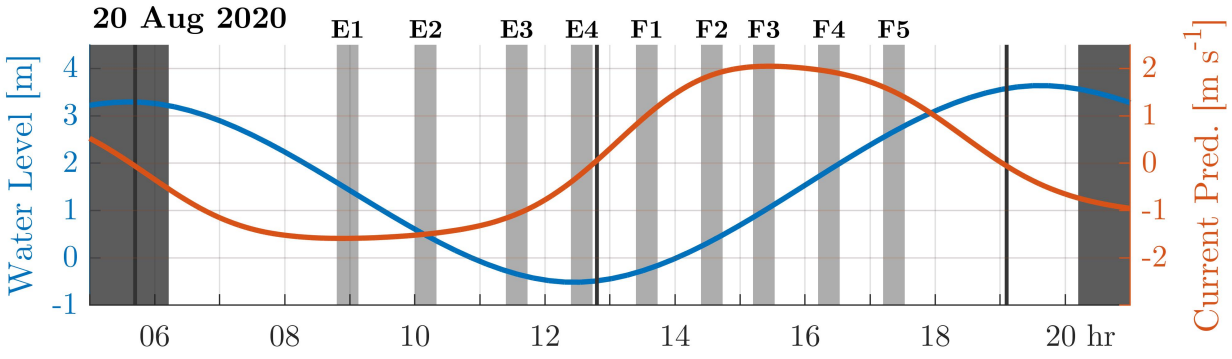

FIG. 3. Predicted water level and tidal currents over the test day. Survey periods are indicated in light grey. Dark grey vertical lines indicate slack tide.

to either hold constant depth or repeatedly profile between the surface and a target depth. Constant depth deployments were intended to provide consistent observational distributions. Profiling deployments were used to ensure along-track localizations by 'bread-crumbing' GPS data in case of poor acoustic connectivity, with the awareness that such a method may smear horizontal velocity measurements vertically through the water column. As the μFloats are prototype instruments, 16 out of 175 total float drifts were rendered invalid due to malfunctions (mechanical, electrical, or software) or human programming errors. Also, roughly 2.5 float drifts were excluded due to suspected float interactions with the seabed, determined by manual review of the IMU data. Consequently, analytical results from each survey cycle consisted of data from 14-18 floats, with the exact number indicated where relevant.

4) WATER PROPERTIES

A hand-deployed Xylem CastAway CTD was used to measure profiles of temperature and salinity. Derived quantities of density and sound speed were also provided by the instrument. One profile was collected during each survey cycle, though position ranged between SK3 and SK2, depending on flow speed and direction. Each cast took about 30 seconds to perform. The sound velocity data at this position was assumed representative of the channel and used to localize all μFloats during the survey cycle.

Accepted for publication in *Journal of Atmospheric and Oceanic Technology*. DOI 10.1175/JTECH-D-22-0034.1.

c. Deployment Layouts and Times

On 20 August 2020, four surveys were performed during ebb tide (E1-E4) and five during flood tide (F1-F5) for a total of nine surveys, each indicated by the grey regions in Figure 3. Surveys were performed by two small vessels (10 m), each with a pilot and two crew members. The μFloats were programmed for underwater survey periods lasting 20 minutes, the approximate time necessary to traverse the region of interest at a speed of 1.5 m s^{-1}. Survey start times were chosen to coincide with the beginning of SWIFT data collection intervals to maximize data overlap in the region of interest. Approximately three minutes prior to the start of the survey period, the vessels performed a coordinated deployment of the drifting devices, following the layout stencils shown in Figure 1c,d. One vessel primarily deployed SWIFTs and upstream SLBs while the other vessel deployed the μFloats and downstream SLBs. For float deployments, the vessel maintained a steady, low speed (3 m s^{-1}), and floats were tossed overboard every 5 s, providing an approximate cross-stream resolution of 15-20 m. For profiling surveys, maximum depths were assigned based on the anticipated cross-channel deployment location and corresponding water depth (accounting for tidal variation in water level). For constant depth surveys, target depths were similarly varied cross-channel: every 3-4 floats were assigned a set of target depths that covered 1 m below the surface to 1 m above the bottom (based on the intended deployment location) in order to resolve cross-stream variation in the vertical velocity gradient. SLBs were deployed around floats with the goal of maintaining robust connectivity of the nanomodems. Based on lessons learned about drift rates and paths during each survey cycle, SLB and SWIFT placements were adjusted to improve correspondence with μFloat tracks. In addition, during two of of the flood tests, an SLB was caught in an eddy and required manual relocation back into the main channel to ensure continued connectivity.

After all instruments were deployed, the first vessel executed the station-keeping ADCP surveys, while the second vessel drifted downstream with the SWIFTs, μFloats, and SLBs. The CTD profiles were also acquired during this drifting period. Once the μFloats resurfaced and the station-keeping measurements were completed, both vessels participated in recovery efforts. Most instruments were found by sight, but locating some μFloats relied on reference to a custom-built cellular-based GPS tracking app. Once all instruments were recovered, they were redistributed to their respective deployment vessel, vessels returned upstream, floats were reprogrammed with a new start time,

Accepted for publication in *Journal of Atmospheric and Oceanic Technology*. DOI 10.1175/JTECH-D-22-0034.1.

and the process began again. Because of the variable time required to recover all the instruments, the interval between surveys was irregular (Figure 3). Recovery and reset during ebb tide typically took longer (~ 1 hour), with some instruments washing ashore on the north side of the channel and requiring assistance from friendly beach walkers, and some traveling out into Port Madison, where larger waves inhibited visual location of the μFloats. During flood tide surveys, most instruments converged within a small area, resulting in faster recovery and reset times (~ 40 min).

d. Data Analysis

To evaluate the effectiveness of μFloat data against SWIFT and station-keeping ADCP data, we compared horizontal velocity measurements across platforms in the following three modes: (1) time-evolution, (2) vertical profiles, and (3) horizontal gradients. Additionally, we used these data to describe the spatial and temporal current variations in Agate Pass.

We examined the mean-flow time-evolution by comparing measurements from all three instrument platforms against the NOAA current prediction (NOAA 2020). NOAA predictions are provided at 2.7 m (9 ft) depth relative to mean-lower-low-water (MLLW) at a location approximately 50 m NE from SK2. NOAA generates these predictions using harmonic analysis (Parker 2007), with constituents derived from a 2015 ADCP deployment at that location (Kammerer et al. 2021). As all instruments sample in a surface-relative coordinate frame, they must be shifted to a MLLW-reference coordinate frame by subtracting the time-varying water level. To compute the water level for each survey cycle, we interpolated the depth relative to MLLW from NOAA bathymetric data (NOAA 2010) at SK2. We then subtracted this nominal depth from the bottom-tracking depths measured by the vessel-keeping ADCP during the survey cycle and calculated the mean to produce the nominal water level for the given survey. This water level was then used to shift sample positions of all platforms to the MLLW-reference frame. For all platforms, SK2 served as the reference location for comparison to the NOAA predictions. For SWIFT data, the nearest profile within 150 m of SK2 was interpolated at 2.7 m depth. For μFloat data, all samples within 50 m horizontal radius of SK2 were binned by depth (0.5 m bin width) and bin averaged to produce a vertical profile. The profile was then linearly interpolated at 2.7 m depth. During slack tide (E4), no μFloat samples were obtained near the NOAA prediction location. Note that for all other inter-platform comparisons, data was left in surface-referenced coordinates.

Accepted for publication in *Journal of Atmospheric and Oceanic Technology*. DOI 10.1175/JTECH-D-22-0034.1.

To examine vertical structure, we compared velocity profiles from all platforms at each station-keeping location, using vessel-mounted ADCP data as reference ground truth. For SWIFT data, the closest profile within 50 m of the station-keeping location was selected. For μFloats, we assembled all 30-second-averaged μFloat data into a three-dimensional distance-weighted interpolation function. We queried the interpolation function at the station-keeping locations at 0.5 m depth intervals from surface to sea-floor. Due to insufficient coverage during ebb deployments, interpolation at SK3 was not possible. To exclude erroneous interpolation near the water surface, the μFloat profiles were clipped to the depth of the shallowest μFloat sample within 100 m.

To extend these comparisons over the entire channel, the μFloat array data was compared to the SWIFT data. The interpolation functions constructed from μFloat data were queried at each SWIFT data point. Median, interquartile range, and interdecile range of the difference between SWIFT and array measurements were computed from all samples in a given survey cycle. The median absolute difference (MAD) serves as the overall figure of merit.

To examine the horizontal distribution of horizontal velocity magnitude, we interpolated the array data at 2 m depth over the entire domain. The nominal horizontal extent of the μFloat samples was identified using MATLABs 'boundary' function, adjusting the 'shrink' parameter to produce a realistic boundary. No extrapolations were made outside this boundary.

To compare the spatial coverage provided by the array relative to the SWIFTs, we computed the horizontal and vertical sample distributions for each platform across all survey cycles. Horizontal coverage was defined as the area within the μFloat sample boundary. Horizontal resolution was computed by spatially binning samples taken by the given platform onto a uniform grid with 100 m resolution and reported as the mean number of unique samples per grid cell. For SWIFTs, one profile was counted as one horizontal sample. Vertical resolution is similarly computed by vertically binning samples in 1 m depth bins and reported as the mean number of samples per bin for the given survey and platform.

3. Results

a. Time Evolution

Figure 4 shows the time evolution of water level (a) and horizontal velocity (b) as compared with NOAA predictions, as well as the observed sound speed (c) and density profiles (d) taken during

Accepted for publication in *Journal of Atmospheric and Oceanic Technology*. DOI 10.1175/JTECH-D-22-0034.1.

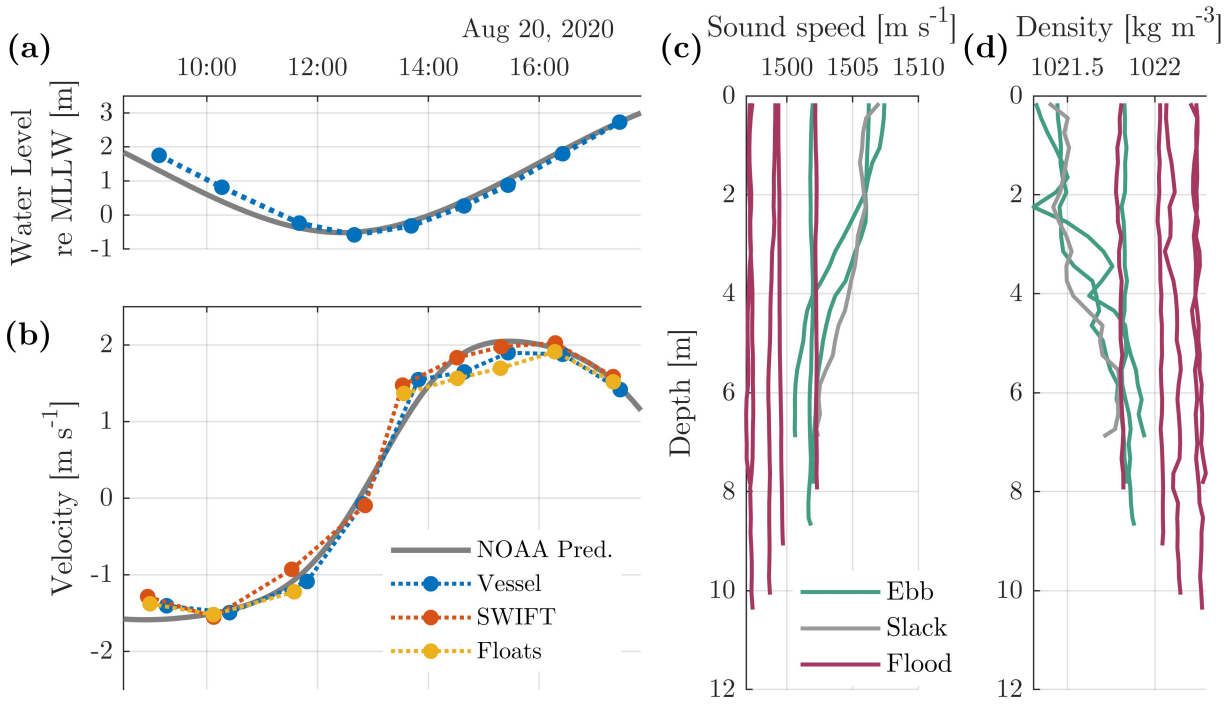

FIG. 4. Time evolution of (a) water level estimated from vessel-keeping ADCP and (b) horizontal velocity measured from all devices, as compared to NOAA prediction. Profiles of sound speed (c) and water density (d) were taken during each survey cycle.

each survey cycle. A phase lag of about 1 hour is evident in both water level and maximum ebb velocity, though not on the flood. Observed water velocity accelerates more quickly on flood than predicted, indicating the presence of a non-harmonic feature of the tidal currents (Parker 2007). This discrepancy relative to the NOAA prediction is unsurprising, given that harmonic analysis inherently removes such features as noise (Parker 2007), and was also observed in prior bottom-mounted ADCP measurements (Wang and Yang 2017). Overall, sound speed and density profiles are consistent in time. The mild sound speed and density gradients on ebb and slack (E4) surveys derive from a slight thermocline (Fig. 4c,d), indicating that the shallower waters of Port Orchard are warmer than Puget Sound. Additionally, the more uniform sound speed profile is favorable for acoustic localizations (i.e., the sound speed profile does not trap SLB localization pings above float depth).

Accepted for publication in *Journal of Atmospheric and Oceanic Technology*. DOI 10.1175/JTECH-D-22-0034.1.

b. Vertical Profiles

Figure 5 depicts the depth-varying water speed at each station-keeping location as a function of time. As typical for open-channel flows, currents are strongest at the surface and diminish with depth. The velocity profiles observed are blunt, with velocities diminishing only 10-25% from surface to near-seabed during all periods excepting slack tide (E4). Qualitatively, the velocity profiles derived from the μFloat data match the SWIFT and vessel-keeping profiles over most sites and surveys (e.g., SK1 during F1-F5 and SK2 during E2 and F2-F4), often within the observed variability at the location. Due to the variable coverage of the drifting platforms, there are insufficient samples within each survey and station-keeping to perform a robust statistical evaluation of patterns of difference between vessel, SWIFT, and μFloat profiles at this local level.

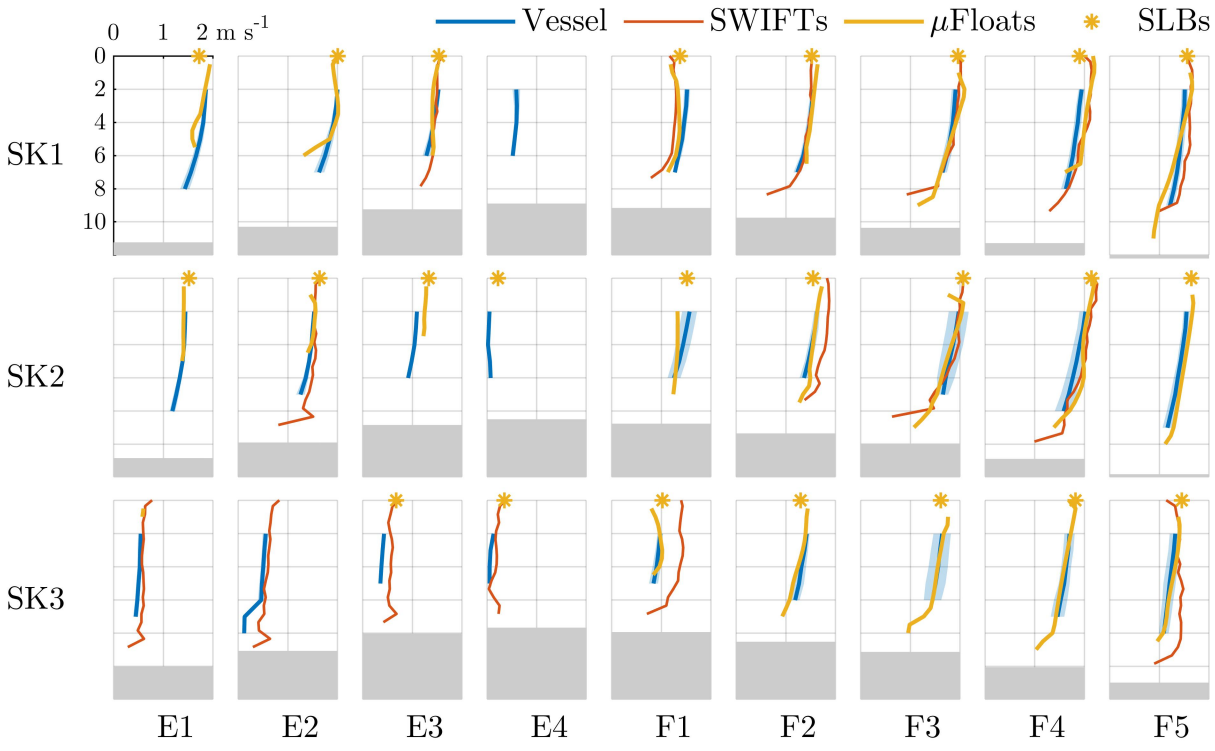

FIG. 5. Current speed vs. depth at each station-keeping location. Variable coverage and deployment locations resulted in insufficient data for float profiles at SK3 during ebb, and all stations at slack (E4), Similarly, SWIFT coverage was insufficient for various surveys and locations. Light blue indicates local variability measured by the station-keeping ADCP and the grey box indicates the water depth at each location and time.

Accepted for publication in *Journal of Atmospheric and Oceanic Technology*. DOI 10.1175/JTECH-D-22-0034.1.

An examination of the difference between SWIFT and float measurements across the all surveys (Figure 6) reveals median absolute deviations (MAD) within about 10% of the nominal velocity (with the exception of slack tide E4, where flow speed is near zero). Additionally, no significant difference is observed between profiling (E1, E3, F1, F3, F5) and depth-tracking (E2, E4, F2, F4) float control modes.

Survey	Speed [m s^{-1}]	nEval	$U_{\mu Float}$ - U_{SWIFT}	MAD [m s^{-1}]	%
E1	1.4	593		0.06	4.3
E2	1.5	638		0.06	4.2
E3	1.1	761		0.07	6.5
E4	0.1	339		0.08	103.1
F1	1.5	1126		0.19	12.0
F2	1.6	1079		0.10	5.8
F3	1.9	968		0.13	6.6
F4	1.9	781		0.22	11.7
F5	1.4	1272		0.11	7.5

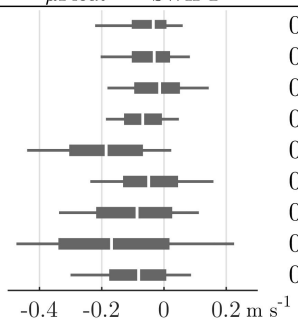

FIG. 6. Horizontal velocity measurement differences (m s^{-1}) between SWIFTs and μFloats over tidal cycle. The white lines, thick grey bars, and thin grey lines indicate median, interquartile range, and interdecile range respectively, evaluated over nEval samples. Percentage difference is Mean Absolute Deviation (MAD) / Speed.

c. Coverage and Resolution

As evident in the profile data, the SWIFTs and μFloats provide variable spatial coverage resulting from changes in deployment distribution and advection trajectories. Figures 7 and 8 offer an inter-platform comparison of float and SWIFT sampling during a representative ebb (E2) and flood (F4) deployment, respectively. Because both SWIFTs and floats were deployed at similar stream-wise locations and distributed evenly across the channel, the across-channel measurement extents are roughly equivalent and the along-channel extents are proportional to the advective velocity (Table 1). While the SWIFTs provide about twice as many samples as the float array (Table 1), they are horizontally sparse. Thus, the float array provides better horizontal resolution than the SWIFTs, as shown in Figure 7a,c and 8a,c. The SWIFTs provide consistent vertical resolution of 0.5 m from surface to the sea floor, with full range up to 20 m (Figs. 7b and 8b). Vertical coverage provided by the floats is less consistent and coarser, with sampling determined either by the set of depths for constant-depth floats (Fig. 7d), or the max depth for profiling floats (Fig. 8d). Profiling mode

Accepted for publication in *Journal of Atmospheric and Oceanic Technology*. DOI 10.1175/JTECH-D-22-0034.1.

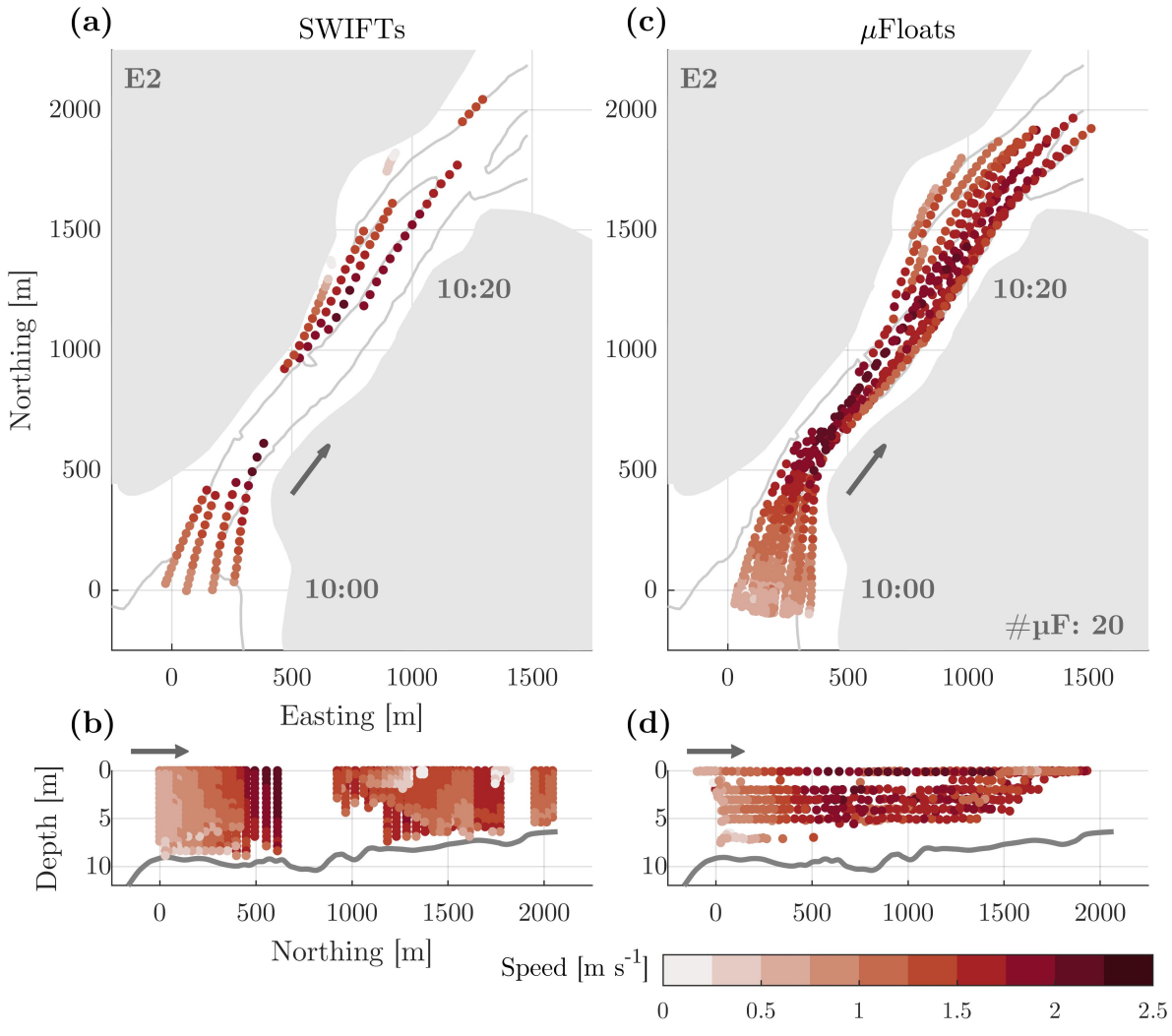

FIG. 7. Distribution of SWIFT (a,b) and float (c,d) samples during E2 deployment. Gaps in SWIFT data occur during onboard processing periods. Floats were programmed to hold constant depth during this survey cycle. Note (b,d) are projected onto the Northing ordinate, with west pointing into the page. The light grey line in (a,c) indicates a 6 m depth contour. The dark grey line in (b,c) indicates bathymetry along the thalweg.

does appear to offer better distribution of vertical samples (Table 1), but may vertically average horizontal velocity in locations with stronger vertical shear than Agate Pass.

d. Horizontal Distribution of Currents

Figure 9 shows the horizontal velocity magnitude at 2 m depth over the domain, as resolved by the float array. During the ebb tide (E2, E3), the flow accelerates as it enters the channel, with peak

Accepted for publication in *Journal of Atmospheric and Oceanic Technology*. DOI 10.1175/JTECH-D-22-0034.1.

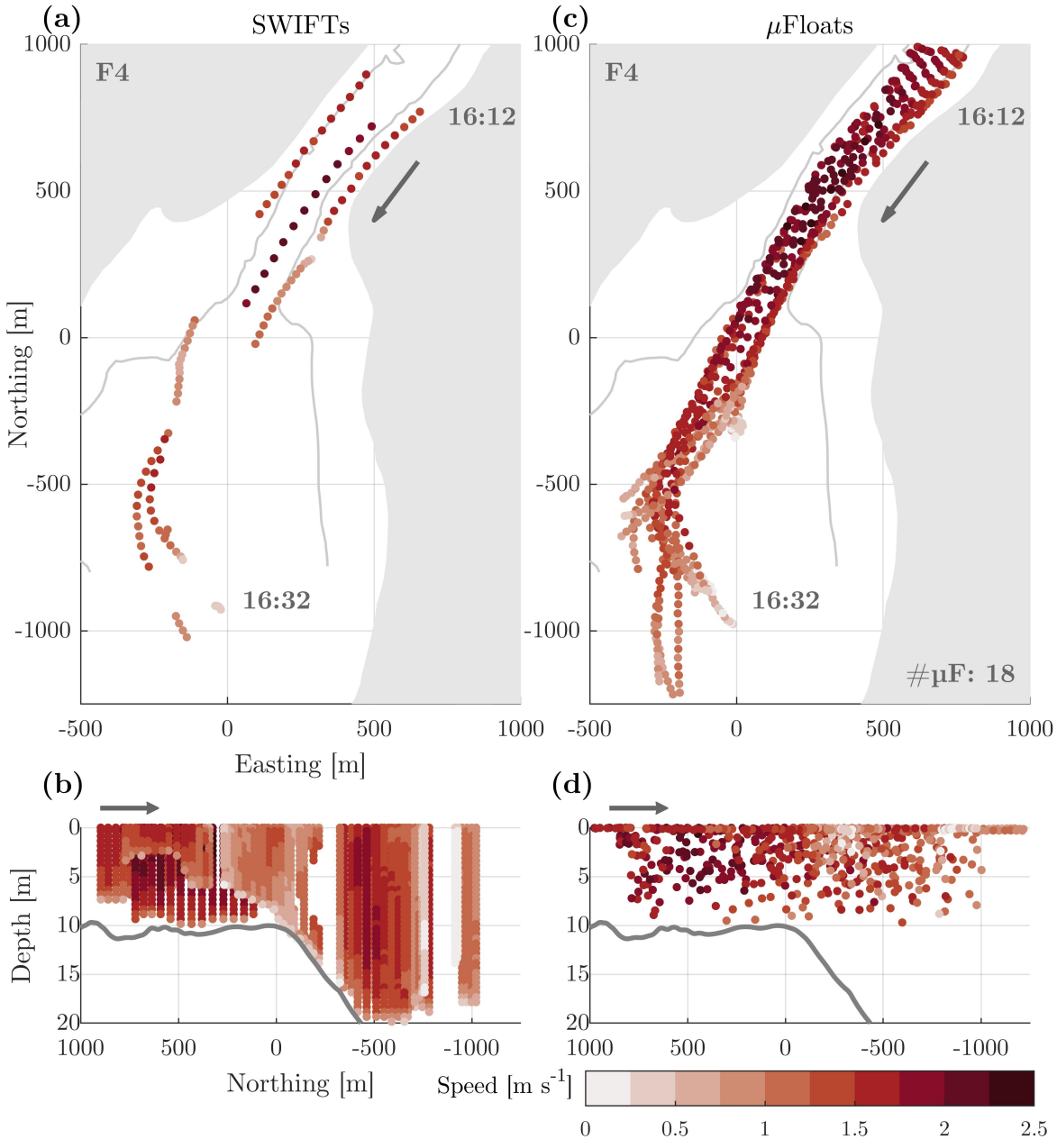

FIG. 8. Distribution of SWIFT (a,b) and float (c,d) samples during F4 deployment. Floats were programmed to profile during this survey. Note (b,d) are projected onto the Northing ordinate, with east pointing into the page. The grey line indicates bathymetry along the thalweg.

currents observed in the center of the channel. On the flood tide (F3, F4), both the distributions (Fig. 9c,d and constituent floats trajectories (e.g., Fig. 8c) reveal a jet exiting the south end of the channel and extending along the thalweg of the bay (for bathymetry, refer to Fig. 1b).

Accepted for publication in *Journal of Atmospheric and Oceanic Technology*. DOI 10.1175/JTECH-D-22-0034.1.

Table 1. Sampling statistics for SWIFTs and μFloats over tidal cycle

			SWIFTs			μFloats			
Tide	Speed	Coverage	Samples	Horz. Res.	Vert. Res.	Samples	Horz. Res.	Vert. Res.	Mode
	m s^{-1}	km^2		#/(100 m)^2	#/1 m		#/(100 m)^2	#/1 m	
E1	1.4	0.51	1619	4	316	639	9	90	Profiling
E2	1.5	0.49	1412	3	277	715	9	72	Constant
E3	1.1	0.33	1419	3	236	720	14	94	Profiling
E4	0.1	0.06	1348	8	246	364	26	57	Constant
F1	1.6	0.33	2257	3	267	617	11	70	Constant
F2	1.7	0.30	2073	3	234	834	13	100	Profiling
F3	1.9	0.38	3184	3	283	691	10	72	Constant
F4	1.9	0.42	2442	2	223	837	11	74	Profiling
F5	1.4	0.33	2472	3	250	610	10	59	Constant

Accepted for publication in *Journal of Atmospheric and Oceanic Technology*. DOI 10.1175/JTECH-D-22-0034.1.

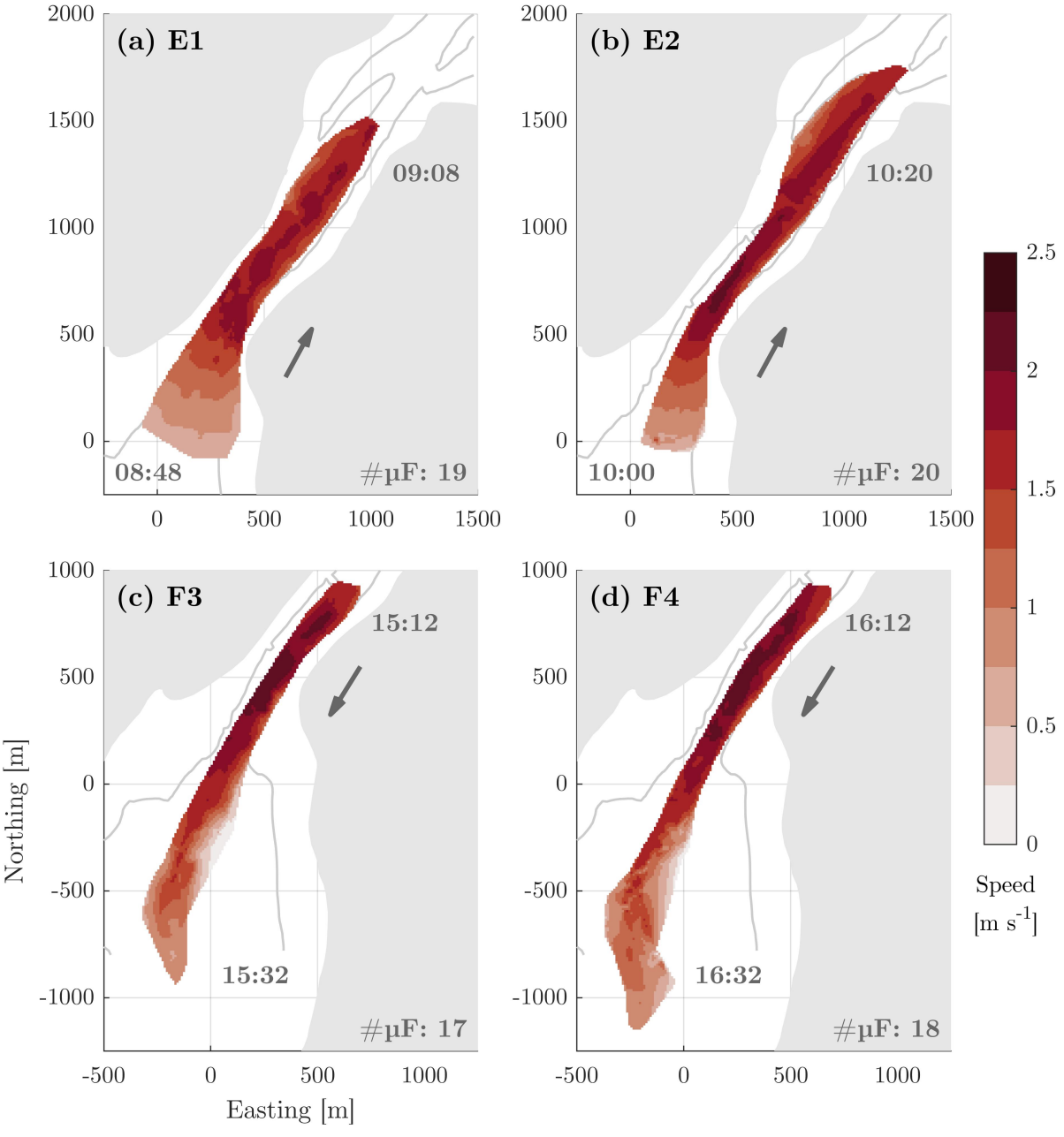

FIG. 9. Horizontal distribution of currents at 2 m depth, as interpolated from μFloat array data, for surveys E1, E2, F3 and F4. The light grey line indicates a 6 m depth contour.

e. Eddies

Examination of the μFloat tracks during F3 and F4 reveal circular trajectories on the southeastern edge of the jet, indicating eddies shed from the jet (Fig. 10). Approximately five minutes after

Accepted for publication in *Journal of Atmospheric and Oceanic Technology*. DOI 10.1175/JTECH-D-22-0034.1.

entering the eddies, the floats began recovery mode, and consequently surfaced and rejoined the primary flow. This behavior, along with the variations in trajectory with float depth (e.g., during F3, the three floats that were entrained in the eddy were at 2, 4, and 5 m) suggests a sub-surface flow feature with depth-varying structure.

4. Discussion

Note that the focus of this experiment was on short duration surveys that captured the spatial structure (horizontal and vertical) of horizontal tidal currents in a small survey area $O(1)$ km.

a. Characteristics of Agate Pass Tidal Currents

The nine surveys provide significant spatial and temporal detail of the tidal current at the south end of Agate Pass, a domain roughly 2 km long and varying from 300 m across the channel to 1 km across Port Orchard.

Since tides here are mixed-semidiurnal, ebb and flood velocities vary considerably throughout the lunar month: a full site characterization would require repeated surveys over multiple days. The surveys presented here only resolved one strong exchange from peak ebb to peak flood. Flow dynamics and the resulting horizontal and vertical gradients for weaker exchanges are expected to be different. As floats may quickly leave the area of interest and thus require near-constant supervision, they are not well-suited for long-duration surveys to extract tidal constituents. Such a task is better suited to bottom-mounted, stationary ADCPs for vertical resolution (McMillan and Hay 2017), shore-mounted X-band radar systems for horizontal resolution (Bell et al. 2012), or Coastal Acoustic Tomography (Kaneko et al. 1994; Elisseeff et al. 1999; Zhang et al. 2017), though the last is better suited to larger scale horizontal structures (5-10 km range, 100 m resolution). A comprehensive characterization of flow conditions could be achieved by collecting distributed samples (such as that from SWIFTs and float arrays) over several days that included a representative range of tidal current magnitudes, and coupling those measurements with continuous, multi-month data from a bottom-mounted ADCP.

Accepted for publication in *Journal of Atmospheric and Oceanic Technology*. DOI 10.1175/JTECH-D-22-0034.1.

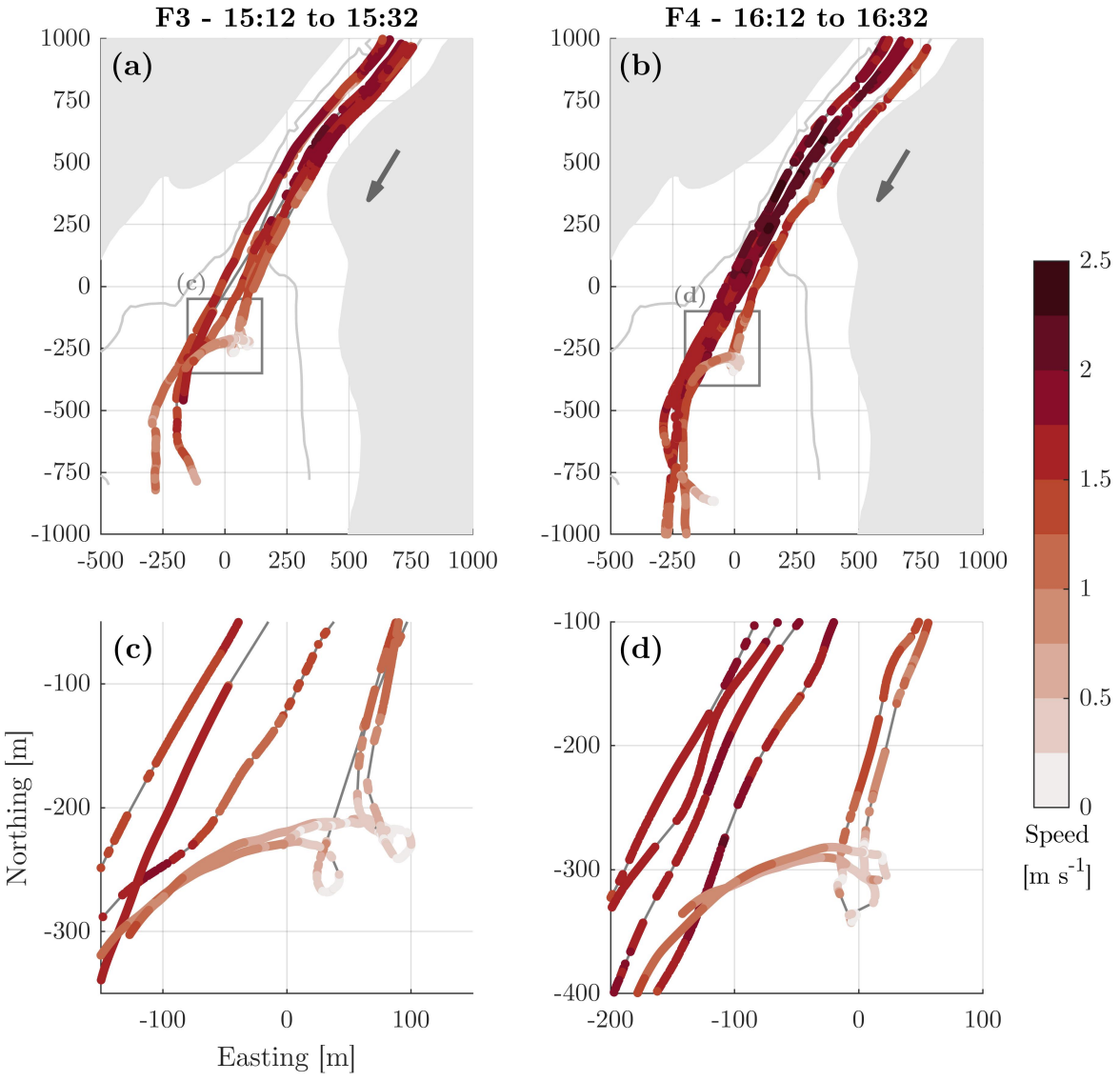

FIG. 10. Float tracks during flood surveys F3 (a) and F4 (b) showed evidence of entrainment in eddies shedding from channel jet. The light grey line indicates a 6 m depth contour. (c) and (d) provide detail of float trajectories in the region of the probable eddy. Only a subset of tracks are shown for clarity and include floats at multiple depths. Note that this is the full-resolution float data, rather than the 30-s averages used for comparison with ADCP data, and dark grey lines connect float positions for visual continuity.

b. Inter-platform Comparison

In general, we see agreement between horizontal water velocity inferred from μFloat trajectories and velocity measured by station-keeping and drifting ADCPs. This suggests that the μFloats

Accepted for publication in *Journal of Atmospheric and Oceanic Technology*. DOI 10.1175/JTECH-D-22-0034.1.

track with the local water movements with negligible relative motion, such that they can provide horizontally- and vertically-distributed measurements of horizontal water velocity with accuracy comparable to ADCPs. Evidence of μFloat Lagrangian behavior is bolstered by individual float tracks that suggest entrainment in depth-varying eddies (Fig. 10). However, since the μFloats are actively controlling depth, they cannot be considered fully Lagrangian, particularly with regards to measuring vertical motion.

The μFloat array provides more economic sampling coverage and horizontal resolution than the four SWIFTs, as the array and SLBs collective cost ($75k) is approximately one quarter that of four SWIFTS ($300k), albeit with some noteable caveats. First, recovery of twenty-five drifting instruments – especially the μFloats which are smaller and harder to see – takes much more time than recovery of four SWIFTs. By deploying only SWIFTs, the inter-survey gaps could be reduced, thus increasing temporal coverage and total samples. Also, SWIFT recovery is not restricted by the pre-programmed time interval (as on the floats), allowing more flexible deployment schedules and locations. Conversely, the floats capture Lagrangian dynamics the ADCPs cannot easily resolve, such as the eddy tracks observed during surveys F2 and F3.

A common concern for Lagrangian sampling methods is convergence of the drifting devices, thus oversampling convergence zones while undersampling divergent zones (e.g., Ohlmann et al. (2017)). The short surveys implemented here avert this problem: the float sample distribution remains strongly correlated to initial position and dive depth, which is directly controlled. Longer deployments may require active manipulation of float positions mid-survey to mitigate uneven sampling.

c. Contributions from SLBs

While the SLBs are necessary for localizing the μFloats, they are themselves surface drifters. Thus, if their motion is Lagrangian, their track data can be combined with the μFloat data to augment array coverage, providing velocity data at the surface that is not captured by the μFloats. To assess this possibility, we evaluated SLB track data in the same manner as SWIFT and μFloats (30-second averages, first-order central-difference) to derive surface velocity estimates and interpolated them at the station-keeping locations (Fig. 5). The results agree with surface velocities measured by the SWIFTs within ± 0.06 m s^{-1} (median absolute difference), suggesting that both devices acted

Accepted for publication in *Journal of Atmospheric and Oceanic Technology*. DOI 10.1175/JTECH-D-22-0034.1.

as Langrangian drifters in the near-surface currents. Such dynamics are not guaranteed due to potential for wind-induced relative motion. The surface expression of the SLBs is large relative to the subsurface expression (~ 1:1 ratio). As a result, even light winds can generate relative velocities between the SLB and surface currents, as was observed in quiescent flow lake tests when benchmarking the μFloat system (Harrison et al. 2022). Thus, SLB tracks can provide additional useful information, though careful consideration of wind effects is critical when integrating SLB and μFloat data. Lastly, given the need to deploy SLBs with the μFloat array, a clear next step would be merging the capabilities of the SWIFTs into the SLBs, thus providing an efficient multiplatform site characterization method.

d. In situ Distributed Array Sampling

As discussed in Harrison et al. (2020), an important benefit of a Lagrangian float array is the potential to obtain *in situ* data that, unlike velocity, cannot be remotely sensed. The μFloats are all equipped with a temperature sensor (Blue Robotics, ±0.1 °C accuracy, 1 s response time). Figure 11 shows the vertical temperature gradients estimated from μFloat data over all surveys. To produce these estimates, we depth-binned the float data at 0.5 m resolution, then performed a distance-weighted average of samples within 100 m of the CTD profile location (e.g., black circles in Fig. 12). The μFloat data match the CTD within ±0.1 ±0.1 °C (median absolute deviation over all samples in Fig. 11), with differences likely attributable to spatial interpolation, given the site exhibits cross-channel gradients of 0.5-1.5°C. Figure 12 displays float trajectories during surveys F2-F5, colored by temperature. These reveal a consistent temperature gradient across the channel, with water cooler on the southern edge and warmer on the northern, which may be indicative of water originating from different locations in Puget Sound. While further benchmarking of μFloat temperature measurements are required, this is a compelling demonstration of distributed array measurements that capture vertical and horizontal gradients of *in situ* properties.

Accepted for publication in *Journal of Atmospheric and Oceanic Technology*. DOI 10.1175/JTECH-D-22-0034.1.

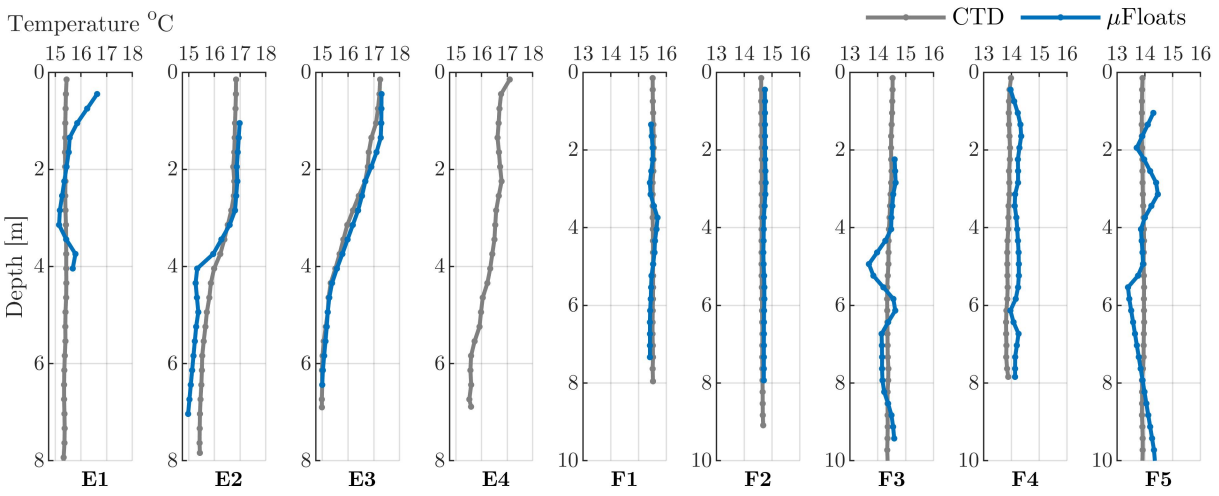

FIG. 11. Temperature profiles estimated from the μFloats relative to CTD measurements.

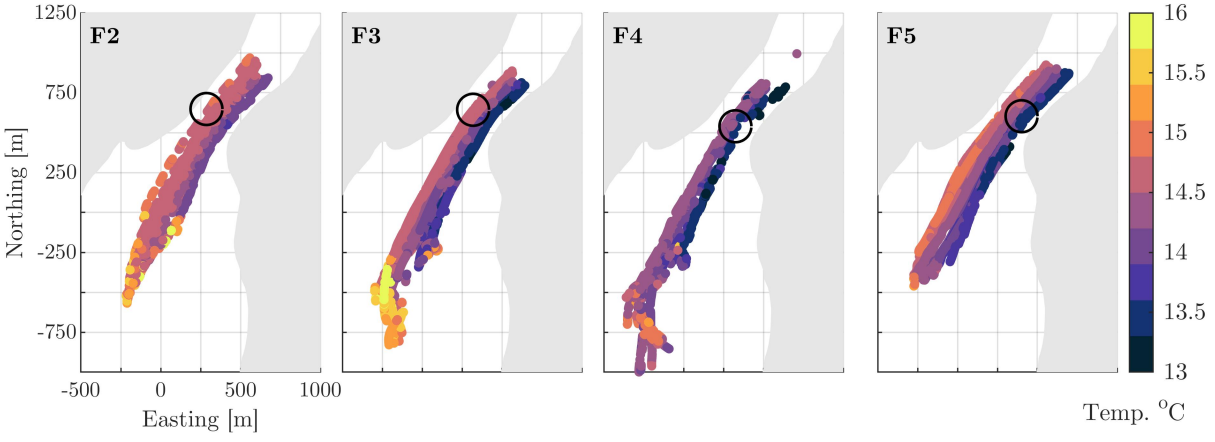

FIG. 12. Horizontal distributions of temperature as measured by the μFloats during surveys F2-F5. Note that float depths vary along the tracks, but temperature during flood is well-mixed vertically, as seen in Fig. 11. Black circles indicate the 100 m boundary for samples used in profile reconstructions in Fig. 11, F2-F5.

Additionally, one μFloat was equipped with a downward facing camera (GoPro Session 5) and LED dive lights for opportunistic benthic composition surveys between SK2 and SK3. The resulting imagery was of variable quality, but did show that bottom composition in the area of the channel with strong currents was primarily scoured to cobble, as expected for high energy sites. A video taken during slack tide east of this region revealed a sandy bottom populated by crabs, starfish, and a few fish – evidence that flow in that area remains low throughout the tidal cycle. However, two control behaviors of the μFloat degrade the quality of benthic surveys. First, the buoyancy engine

Accepted for publication in *Journal of Atmospheric and Oceanic Technology*. DOI 10.1175/JTECH-D-22-0034.1.

motor induces considerable rotational motion while holding depth. Second, because the float holds constant depth, the relative distance to bottom is difficult to assess and the size of objects on the bottom is ambiguous. Addition of an altimeter, as implemented by Roman et al. (2011), would improve these results, as would a control algorithm that reduces actuation. Additional details are available in the Supplementary Materials.

5. Conclusion

Here, we have described the first tidal channel deployment of the μFloat array in Agate Pass, WA over a series of nine survey cycles performed from ebb to flood, during which maximum observed currents exceeded 2 m s^{-1}. While the hydrodynamics of Agate Pass are not scientifically novel, the results are technologically compelling. Measurements of horizontal velocity magnitude derived from the μFloats matched those from the four drifting SWIFT ADCPs to within 10% of the nominal flow speed. The array was also able to resolve vertical gradients in agreement with those measured by stationary and drifting ADCPs, while providing 2-4 times the horizontal resolution of the drifting ADCPs over the same region, all with lower instrument cost. Additionally, the μFloats provided *in situ* temperature measurements that approximately matched those from CTD profiles and were able to resolve strong horizontal gradients. This suggests that low-cost, coastal floats are capable of gathering scientifically relevant data in energetic flows. The potential benefits extend beyond current measurements demonstrated here: as a modular platform, the μFloats can be adapted to measure salinity, dissolved oxygen, turbidity, or underwater sound. Such spatially and temporally resolved measurements would significantly enhance our ability to resolve a variety of physical, biological, and chemical conditions and processes in coastal waters.

Acknowledgments. The authors would like to acknowledge Alex de Klerk, E.J. Rainville, and Zachary Tully for providing essential help during the Agate Pass field work. All colormaps used here came from the **cmocean** library (Thyng et al. 2016). We also thank three anonymous reviewers for their thoughtful feedback.

Funding: The μFloat was developed based upon funds from NSF Graduate Research Fellowship (DGE-1762114) and array construction supported by ONR DURIP (N00014-17-1-2336). Agate Pass field work was funded by the U.S. DoD Naval Facilities Engineering Command (N0002410D6318 / N0002418F8702). The authors have no conflicts of interest to disclose.

Data availability statement. The data and software supporting this work are openly available in University of Washington - ResearchWorks Archive at `http://hdl.handle.net/1773/48360`.

References

An, E., M. R. Dhanak, L. K. Shay, S. Smith, and J. Van Leer, 2001: Coastal Oceanography Using a Small AUV. *Journal of Atmospheric and Oceanic Technology*, **18 (1)**, 215–234, https://doi.org/10.1175/1520-0426(2001)018⟨0215:COUASA⟩2.0.CO;2.

Bell, P. S., J. Lawrence, and J. V. Norris, 2012: Determining currents from marine radar data in an extreme current environment at a tidal energy test site. *International Geoscience and Remote Sensing Symposium (IGARSS)*, 7647–7650, https://doi.org/10.1109/IGARSS.2012.6351856.

Blunden, L., and A. Bahaj, 2007: Tidal energy resource assessment for tidal stream generators. *Proceedings of the Institution of Mechanical Engineers, Part A: Journal of Power and Energy*, **221 (2)**, 137–146.

Brown, J., C. Tuggle, J. MacMahan, and A. Reniers, 2011: The use of autonomous vehicles for spatially measuring mean velocity profiles in rivers and estuaries. *Intelligent Service Robotics*, **4 (4)**, 233–244, https://doi.org/10.1007/s11370-011-0095-6.

Chen, C., S. Shiotani, and K. Sasa, 2013: Numerical ship navigation based on weather and ocean simulation. *Ocean Engineering*, **69**, 44–53.

Cheng, R. T., and R. E. Smith, 1998: A nowcast model for tides and tidal currents in san francisco bay, california. *Ocean Community Conference, Baltimore, USA*, Citeseer.

Defne, Z., and N. K. Ganju, 2015: Quantifying the residence time and flushing characteristics of a shallow, back-barrier estuary: Application of hydrodynamic and particle tracking models. *Estuaries and Coasts*, **38 (5)**, 1719–1734.

Deppe, R. W., J. Thomson, B. Polagye, and C. Krembs, 2013: Hypoxic intrusions to puget sound from the ocean. *2013 OCEANS-San Diego*, IEEE, 1–9.

Dickey, T., A. J. Plueddemann, and R. A. Weller, 1998: Current and water property measurements in the coastal ocean. *The Sea*, K. H. Brink, and A. R. Robinson, Eds., Vol. 10, John Wiley & Sons, Inc., 367–398.

Elisseeff, P., H. Schmidt, M. Johnson, D. Herold, N. R. Chapman, and M. M. McDonald, 1999: Acoustic tomography of a coastal front in haro strait, british columbia. *The Journal of the Acoustical Society of America*, **106 (1)**, 169–184, https://doi.org/10.1121/1.427046, URL https://doi.org/10.1121/1.427046, https://doi.org/10.1121/1.42746.

Fenucci, D., A. Munafo, A. B. Phillips, J. Neasham, N. Gold, J. Sitbon, I. Vincent, and T. Sloane, 2018: Development of smart networks for navigation in dynamic underwater environments. *2018 IEEE/OES Autonomous Underwater Vehicle Workshop (AUV)*, IEEE, 1–6.

Fong, D. A., and S. G. Monismith, 2004: Evaluation of the accuracy of a ship-mounted, bottom-tracking adcp in a near-shore coastal flow. *Journal of Atmospheric and Oceanic Technology*, **21 (7)**, 1121–1128, https://doi.org/10.1175/1520-0426(2004)021⟨1121:EOTAOA⟩2.0.CO;2.

Foreman, M. G., W. R. Crawford, and R. F. Marsden, 1995: De-tiding: Theory and practice. *Coastal and estuarine studies*, 203–203.

Garwood, J. C., A. J. Lucas, P. Naughton, M. H. Alford, P. L. D. Roberts, J. S. Jaffe, L. DeGelleke, and P. J. S. Franks, 2020: A novel cross-shore transport mechanism revealed by subsurface, robotic larval mimics: Internal wave deformation of the background velocity field. *Limnology and Oceanography*, **65 (7)**, 1456–1470, URL https://onlinelibrary.wiley.com/doi/10.1002/lno.11400.

Geyer, W. R., and R. Signell, 1990: Measurements of tidal flow around a headland with a shipboard acoustic Doppler current profiler. *Journal of Geophysical Research*, **95 (C3)**, 3189, https://doi.org/10.1029/JC095iC03p03189.

Godin, G., 1983: On the predictability of currents. *The International Hydrographic Review*.

Gould, W. J., 2005: From swallow floats to argo—the development of neutrally buoyant floats. *Deep Sea Research Part II: Topical Studies in Oceanography*, **52 (3-4)**, 529–543.

Guerra, M., R. Cienfuegos, J. Thomson, and L. Suarez, 2017: Tidal energy resource characterization in chacao channel, chile. *International journal of marine energy*, **20**, 1–16.

Guerra, M., A. E. Hay, R. Karsten, G. Trowse, and R. A. Cheel, 2021: Turbulent flow mapping in a high-flow tidal channel using mobile acoustic doppler current profilers. *Renewable Energy*, **177**, 759–772, https://doi.org/https://doi.org/10.1016/j.renene.2021.05.133.

Guerra, M., and J. Thomson, 2016: ORPC RivGen Wake Characterization. *Marine Energy Technology Symposium*, Washington, D.C.

Guerra, M., and J. Thomson, 2017: Turbulence measurements from five-beam acoustic doppler current profilers. *Journal of Atmospheric and Oceanic Technology*, **34 (6)**, 1267–1284, https://doi.org/10.1175/JTECH-D-16-0148.1.

Harrison, T., K. M. Thyng, and B. Polagye, 2020: Comparative evaluation of volumetric current measurements in a tidally dominated coastal setting: A virtual field experiment. *Journal of Atmospheric and Oceanic Technology*, **37 (4)**, 533–552, https://doi.org/10.1175/JTECH-D-19-0131.1.

Harrison, T., and Coauthors, 2022: Adaptable swarm sensing in coastal waters: Design and performance of the μfloat system. *Under review; archived at Earth and Space Science Open Archive*, 37, URL https://doi.org/10.1002/essoar.10510276.1.

Heitsenrether, R., L. Fiorentino, D. W. Velasco, and W. D. Wilson, 2018: Evaluating performance of acoustic current profiler sensor on small, dynamic surface buoy. *OCEANS 2018 MTS/IEEE Charleston*, 1–8, https://doi.org/10.1109/OCEANS.2018.8604697.

Jaffe, J. S., P. J. S. Franks, P. L. D. Roberts, D. Mirza, C. Schurgers, R. Kastner, and A. Boch, 2017: A swarm of autonomous miniature underwater robot drifters for exploring submesoscale ocean dynamics. *Nature Communications*, **8**, 1–8, https://doi.org/10.1038/ncomms14189.

Jayne, S. R., D. Roemmich, N. Zilberman, S. C. Riser, K. S. Johnson, G. C. Johnson, and S. R. Piotrowicz, 2017: The argo program: Present and future. *Oceanography*, **30 (2)**, 18–28, URL http://www.jstor.org/stable/26201840.

Jin, G., H. Pan, Q. Zhang, X. Lv, W. Zhao, and Y. Gao, 2018: Determination of harmonic parameters with temporal variations: An enhanced harmonic analysis algorithm and application to internal tidal currents in the south china sea. *Journal of atmospheric and oceanic technology*, **35 (7)**, 1375–1398.

Kammerer, C., G. Dusek, L. Heilman, K. Kirk, and C. Paternostro, 2021: Puget sound current survey 2015-2017, including the united states' portions of the greater salish sea.

Kaneko, A., G. Yuan, N. Gohda, and I. Nakano, 1994: Optimum design of the ocean acoustic tomography system for the sea of japan. *Journal of Oceanography*, **50 (3)**, 281–293.

Livingston, R. J., 2000: *Eutrophication processes in coastal systems: origin and succession of plankton blooms and effects on secondary production in Gulf Coast estuaries*. CRC press.

Lu, Y., and R. G. Lueck, 1999: Using a broadband adcp in a tidal channel. part i: Mean flow and shear. *Journal of Atmospheric and Oceanic Technology*, **16 (11)**, 1556–1567.

Mahadevan, A., 2016: The impact of submesoscale physics on primary productivity of plankton. *Annual review of marine science*, **8**, 161–184.

Mayer, D. A., J. I. Virmani, and R. H. Weisberg, 2007: Velocity comparisons from upward and downward acoustic doppler current profilers on the west florida shelf. *Journal of Atmospheric and Oceanic Technology*, **24 (11)**, 1950–1960.

McCaffrey, K., B. Fox-Kemper, P. E. Hamlington, and J. Thomson, 2015: Characterization of turbulence anisotropy, coherence, and intermittency at a prospective tidal energy site: Observational data analysis. *Renewable Energy*, **76**, 441–453, https://doi.org/10.1016/j.renene.2014.11.063.

McGilvray, B., and C. Roman, 2010: Control system performance and efficiency for a mid-depth lagrangian profiling float. *IEEE OCEANS 2010 - SYDNEY*.

McMillan, J. M., and A. E. Hay, 2017: Spectral and structure function estimates of turbulence dissipation rates in a high-flow tidal channel using broadband adcps. *Journal of Atmospheric and Oceanic Technology*, **34 (1)**, 5 – 20, https://doi.org/10.1175/JTECH-D-16-0131.1.

Mullison, J., D. Symonds, and N. Trenaman, 2011: ADCP data collected from a liquid robotics Wave Glider. *2011 IEEE/OES/CWTM 10th Working Conference on Current, Waves and Turbulence Measurement, CWTM 2011*, 266–272, https://doi.org/10.1109/CWTM.2011.5759563.

Muste, M., K. Yu, and M. Spasojevic, 2004: Practical aspects of adcp data use for quantification of mean river flow characteristics; part i: moving-vessel measurements. *Flow Measurement and Instrumentation*, **15 (1)**, 1–16, https://doi.org/https://doi.org/10.1016/j.flowmeasinst.2003.09.001.

Neasham, J., 2018: Usmart project website. Accessed May 2021, https://research.ncl.ac.uk/usmart/.

NOAA, 2010: Nos hydrographic survey - h12216. bathymetric data. Accessed August 4, 2020, https://www.ngdc.noaa.gov/nos/H12001-H14000/H12216.html.

NOAA, 2020: Tidal current predictions. pug1501 agate passage, south end; depth: 9 feet. 2020-08-19 to 2020-08-21. Accessed August 4, 2020, https://tidesandcurrents.noaa.gov/noaacurrents/Predictions?id=PUG1501_6.

Norrdine, A., 2012: An algebraic solution to the multilateration problem. *2012 International Conference on Indoor Positioning and Indoor Navigation*.

Ohlmann, J. C., M. J. Molemaker, B. Baschek, B. Holt, G. Marmorino, and G. Smith, 2017: Drifter observations of submesoscale flow kinematics in the coastal ocean. *Geophysical Research Letters*, **44 (1)**, 330–337, https://doi.org/https://doi.org/10.1002/2016GL071537, URL https://agupubs.onlinelibrary.wiley.com/doi/abs/10.1002/2016GL071537.

Palodichuk, M., B. Polagye, and J. Thomson, 2013: Resource mapping at tidal energy sites. *IEEE Journal of Oceanic Engineering*, **38 (3)**, 433–446, https://doi.org/10.1109/JOE.2012.2227578.

Parker, B. B., 2007: Tidal analysis and prediction.

Polagye, B., and J. Thomson, 2013: Tidal energy resource characterization: methodology and field study in Admiralty Inlet, Puget Sound, WA (USA). *Proceedings of the Institution of Mechanical Engineers, Part A: Journal of Power and Energy*, **227 (3)**, 352–367, https://doi.org/10.1177/0957650912470081.

Roman, C., G. Inglis, and B. McGilvray, 2011: Lagrangian floats as sea floor imaging platforms. *Continental Shelf Research*, **31 (15)**, 1592–1598, https://doi.org/10.1016/j.csr.2011.06.019.

Shcherbina, A. Y., E. A. D'Asaro, and S. Nylund, 2018: Observing finescale oceanic velocity structure with an autonomous nortek acoustic doppler current profiler. *Journal of Atmospheric and Oceanic Technology*, **35 (2)**, 411–427, https://doi.org/10.1175/JTECH-D-17-0108.1.

Teledyne RDI, 2019: Acoustic Doppler current profiler: Principles of operation, a practical primer. Teledyne RD Instruments, Poway, CA, 48 pp.

Thomson, J., 2012: Wave breaking dissipation observed with SWIFT drifters. *Journal of Atmospheric and Oceanic Technology*, **29 (12)**, 1866–1882.

Thomson, J., and Coauthors, 2019: A new version of the swift platform for waves, currents, and turbulence in the ocean surface layer. *2019 IEEE/OES Twelfth Current, Waves and Turbulence Measurement (CWTM)*, 1–7.

Thyng, K. M., C. A. Greene, R. D. Hetland, H. M. Zimmerle, and S. F. DiMarco, 2016: True colors of oceanography: Guidelines for effective and accurate colormap selection. *Oceanography*, **29 (3)**, 9–13, https://doi.org/10.5670/oceanog.2016.66.

Todd, R. E., D. L. Rudnick, J. T. Sherman, W. Brechner Owens, and L. George, 2017: Absolute velocity estimates from autonomous underwater gliders equipped with doppler current profilers. *Journal of Atmospheric and Oceanic Technology*, **34 (2)**, 309–333, https://doi.org/10.1175/JTECH-D-16-0156.1.

Velasco, D. W., and S. Nylund, 2019: Performance improvement for adcps on surface buoys. *2019 IEEE/OES Twelfth Current, Waves and Turbulence Measurement (CWTM)*, 1–7.

Wang, T., and Z. Yang, 2017: A modeling study of tidal energy extraction and the associated impact on tidal circulation in a multi-inlet bay system of puget sound. *Renewable Energy*, **114**, 204–214.

Willcox, J. S., J. G. Bellingham, Y. Zhang, and A. B. Baggeroer, 2001: Performance metrics for oceanographic surveys with autonomous underwater vehicles. *IEEE Journal of Oceanic Engineering*, **26 (4)**, 711–725, https://doi.org/10.1109/48.972114.

Zhang, C., and Coauthors, 2017: High-precision measurement of tidal current structures using coastal acoustic tomography. *Estuarine, Coastal and Shelf Science*, **193**, 12–24, https://doi.org/https://doi.org/10.1016/j.ecss.2017.05.014, URL https://www.sciencedirect.com/science/article/pii/S0272771416304851.